USING PALSAR IMAGERY FOR CHARACTERIZING VOLCANIC FISSURES (DYKES) IN THE ETHIOPIAN VOLCANIC PROVINCE

Daniel Mège

Laboratoire de planétologie et géodynamique, UMR CNRS 6112, Université de Nantes,
2 rue de la houssinière, BP 92208, 44322 Nantes, France, Email: daniel.mege@univ-nantes.fr

ABSTRACT

Palsar images are used to delineate and identify dykes in the western Ethiopian volcanic province. Dykes are vertical, fractured solidified magma sheets that play a major role in groundwater storage, and might be considered as potential drilling sites for water supply to the local inhabitants. On Palsar imagery, they can be discriminated from other linear patterns by roughness contrasts between the dyke and its debris slopes and between the debris slopes and the surrounding smooth plain. For an appropriate combination of incidence angle and polarization, dyke signal on Palsar imagery is therefore made of 3 parallel bands of distinct roughness, with the debris slopes appearing brighter than both the dyke and the surrounding plain.

In comparison, multispectral images are good at identifying vegetated dyke portions, but not at tracing dyke continuity. Moreover, uncertainty frequently remains as to the discrimination between dykes and other lienear patterns. Envisat/Asar (band C) and SIR-C (bands C and L) images are very good at identifying dyke continuity, but not at identifying the 3 diagnostic roughness bands, more because of coarser resolution than for incidence angle, beam wavelength, or polarization issues.

The ideal sensor for dyke identification will have a resolution higher than Palsar because still many dykes are too small to be observed by Palsar, a 4-pol mode because the dyke signal is always a trade-off between roughness, vegetation and moisture, and a combination of wavelength (C or L) and incidence angle (20-50°) that is flexible enough to image roughness at a scale of 5 to 100 cm.

1. INTRODUCTION

In the large igneous provinces, magma is transmitted from chambers at depth to flows at surface through large dyke swarms. In the 30 Ma-old Ethiopian volcanic province, the largest dyke swarms are observed in northwestern Ethiopia [1] (Fig. 1). They cover a surface area estimated to be 20,000 km^2 at least. It is presently almost devoid of roads, and from the available imagery the total number of dykes is estimated to be several hundreds. Remote sensing is consequently mandatory for any investigations in this area.

Dyke swarm studies are useful not only for palinspastic plate tectonics and paleostress reconstructions (e.g., [1]), but also for understanding some of the past global climate changes and mass extinctions [2, 3], and for their groundwater storage capabilities [4, 5].

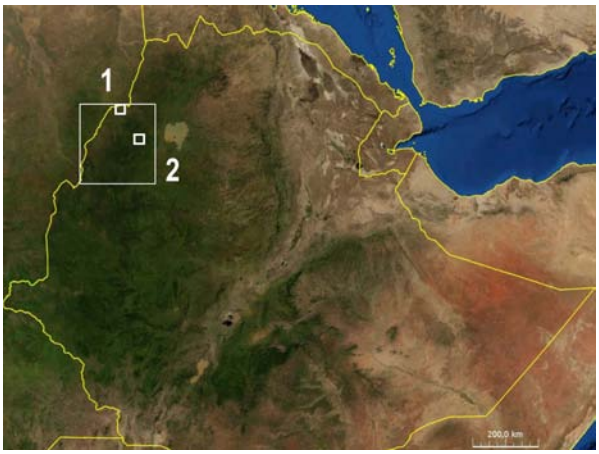

Figure 1. Location of the dyke swarms of northwestern Ethiopia, also corresponding to the study area of ESA/ALOS project ID 3561 (large box), and location of the basaltic (#1) and silicic (#2) dykes investigated in this study.

Most dykes in western Ethiopia are observed at the base level of the volcanic trap series, and most of them have the same basaltic composition as their host rock [6]. For this reason, their topography is usually positive, but not higher than a few meters, and their reflectance is not significantly different for the reflectance of their host rock. Consequently, they are not easily identified on panchromatic images, and on multispectral images they are hardly identified when they are not underlined by a specific vegetation line grown owing to the dyke water content at depth. Many dykes, however, *are actually observed* on most of these datasets, but the issue is that they are observed as lineaments that have no distinctive characters compared to other linear features such as roads, cattle and foot trails, field boundaries, faults, tension fractures, and other anthropic and natural lines. Orbital radar sensors older than Palsar have a coarser resolution, and although a number of dykes are observed, they cannot be interpreted as such either for

Proc. of 'ALOS PI 2008 Symposium", Island of Rhodes, Greece
3–7 November 2008, (ESA SP-664, January 2009)

similar reasons. Here I show that the roughness contrast between a dyke, its debris slopes, and the surrounding ethio-sudanese plain, has a unequivocal signal that can be detected on Palsar multilook images.

2. DYKE SURFACE PROPERTIES

The dykes in the study area have several surface properties that can significantly contribute to radar backscatter. However, as explained below, roughness contrasts offer the most promising potentiality for discriminating dykes and other lineaments.

Figure 2. Basaltic dyke in northwestern Ethiopia, east of the village of Farshewa [5]

2.1. Thickness and length

Dyke thickness is between less than one meter and 20 meters. Dyke thickness is governed by the tensile strength of the host rock, and also the magma viscosity during its emplacement in the dyke fracture, which explains that most thick dykes are silicic [7]. Length is related to thickness by the formula [8, 9]:

$$D_{max}=\frac{K_{IC}(1-\nu^2)}{E}\frac{\sqrt{8}}{\sqrt{\pi}}\sqrt{L} \qquad (1)$$

where D_{max} is displacement (=thickness), K_{IC} is host rock fracture toughness, ν is Poisson's ratio, E the Young's modulus of the host rock, and L is length, which from field work on the dyke population in the study area equals the relation [8]:

$$D_{max} = 0.09L^{0.48} \qquad (2)$$

The cumulated distribution of dyke length follows a power law with an exponent of -1.8 [6], meaning that most dykes are less than a few meters thick. Palsar modes quad-pol, FBS, and FBD, are therefore expected to have a resolution that is sufficient for imaging many dykes, but not all.

2.2. Topography

Most dykes are basaltic within a basaltic host rock. The dyke margins usually form a positive, vertical to nearly vertical relief that rarely exceed a few meters (Fig. 2). In contrast, the silicic dykes, which are less prone to erosion than basalt under the present climate of western Ethiopia, form prominent reliefs (Fig. 3).

2.3. Vegetation

Water storage by basaltic dykes due to pervasive dyke fracturing explains that portions of some of them are underlined by a vegetation line. This explains that these dyke portions are easily identified on multispectral imagery, and suggests that they should also contribute to radar backscatter, in a proportion that depends on the dyke and on the season, wet or dry.

2.4. Roughness

Dyke fracturing is inherent to dyke emplacement. It is acquired by magma cooling, which produces retraction joints whose geometry and spacing depends on the magma cooling conditions [10]. Jointing defines a complex three-dimensional network that cuts the dyke up into prisms. Local tectonic events may add new fractures to the cooling joints. Dyke alteration widens and weakens the fractures, at the surface the prismatic dykes gradually transform to an unstable pile of blocks, whose gravitational destabilization results in blocks falling and breaking up on the ground on both dyke sides, forming a debris slope of dimensions proportional to the dyke thickness and tallness (Figs. 2 and 3). Further alteration and vegetation growth on debris slope decreases block size further.

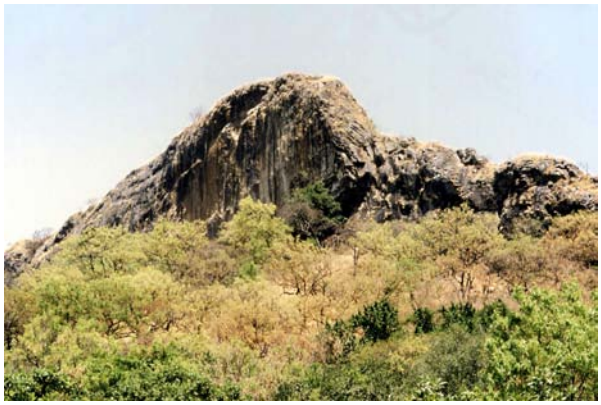

Figure 3. The Serpent dyke, the largest (silicic) dyke of the study area [6], of thickness 20 m

The plain area surrounding the dykes is made of the basal level of the Trap Series. Due to basalt alteration to clay minerals under the present climate conditions, the texture of the plain is smoother than that of the debris slopes. It is therefore expected that the dykes are surrounded by 4 parallel roughness boundaries on radar imagery if the resolution permits: the 2 dyke/debris slope boundaries, and the 2 debris slope/plain boundaries. Identification of such a series of roughness contrasts along dykes would constitute a powerful

criterion for distinguishing dykes fom other linear features observed on the ground by satellites.

3. DYKE #1

This section focuses on a dyke identified in the field in 2008 near the village of Mendoka at the ethio-sudanese border (Fig. 1). The basaltic Mendoka dyke (Fig. 4) is the westernmost dyke ever identified to date in the Ethiopian volcanic province, and broadens the known feeding zone of the traps to the West by 100 km.

Figure 4. View of the Mendoka dyke toward the East. The dyke is on the left, the debris slope on the middle, and the plain on the right.

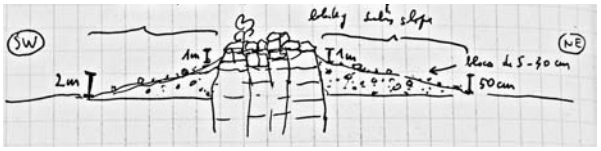

Figure 5. Field cross-section of the Mendoka dyke

Figure 6. Example of terrain around the Mendoka dyke

The thickness of the Mendoka dyke could be estimated to be 5-6 m in the field, but its length could not be measured. Dyke orientation is N125°E. The size of the blocks at the dyke summital surface is within the range 50-100 cm, whereas block size on the debris slopes is within the range 5-30 cm (Figs. 4 and 5).

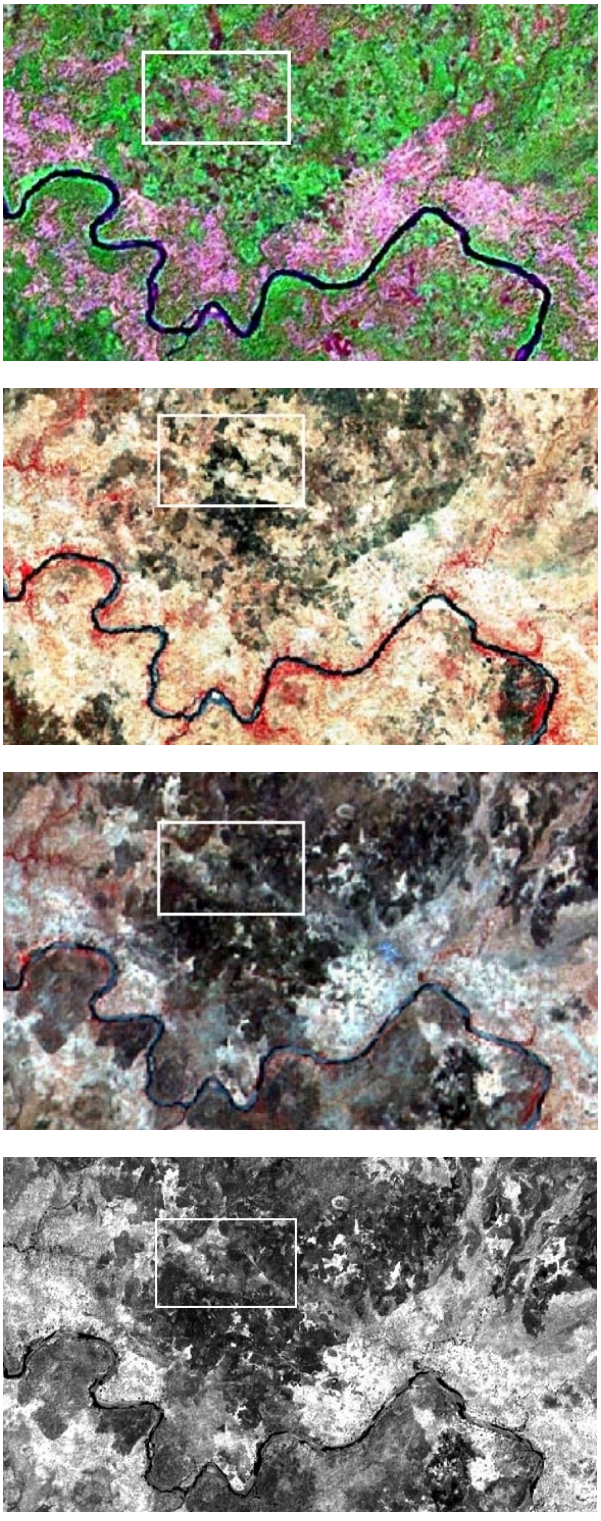

Figure 7. The Mendoka dyke area (white box) as seen during the wet season by Landsat ETM+ (GLCF Geocover 2000, 15m/pixel), and during the dry season by ASTER (bands 321, 15 m/pixel), Spot XS (20 m/pixel), and Spot P (10m/pixel).

How the Mendoka dyke is imaged on multispectral, panchromatic, Envisat/ASAR, and Alos/PALSAR data is displayed on Figs. 7-14. The white box shows the

location of the Mendoka dyke at the field observation site. The length of the diagonal line of the box is 2 km. For every image is given the polarization if relevant, the season, the incidence angle θ, and the nominal resolution.

On multispectral and panchromatic images (Fig. 7), the orientation of the Mendoka dyke is parallel to a trend that is more or less perceptible, but there is no clear evidence of any dyke. On Spot imagery, the dyke is only a weakly prononced alignment of pixels surrounded by trails that are parallel to the dyke —and are actually responsible for the observed trend (Fig. 8).

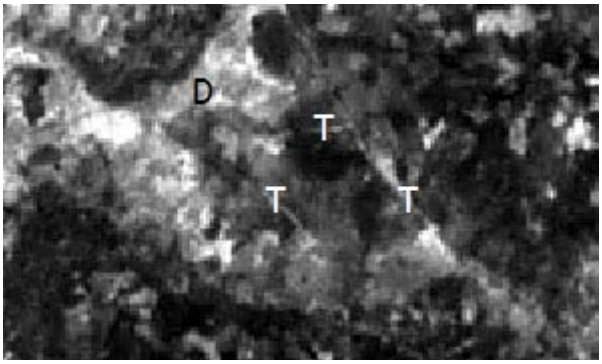

Figure 8. Spot P image of the area in the white box on Fig. 7. T: trail; D: dyke

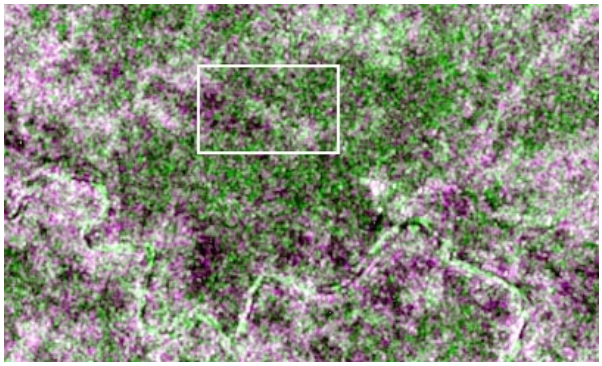

Figure 9. Envisat/ASAR image of the Mendoka area. Red: HH, green: HV, blue: HH/HV. Length of box diagonal line: 2 km. Dry season, θ = 31-36°, 30m/pixel

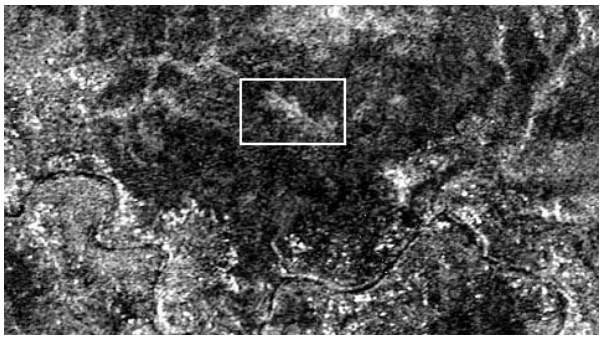

*Figure 10. PALSAR 4-POL image of the Mendoka dyke, HH polarization. Length of box diagonal line: 2 km. Dry season, θ = 21.5°, 30*10 m/pixel*

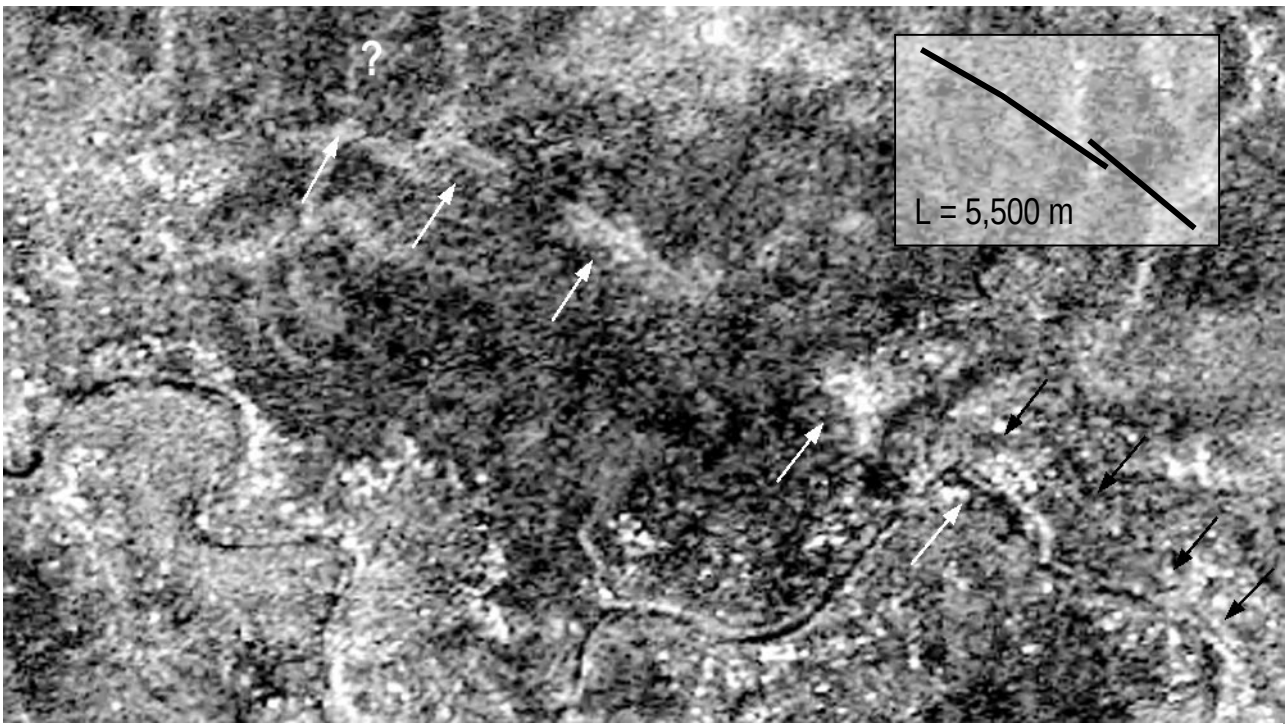

*Figure 11. PALSAR 4-POL HH*VV image of the Mendoka dyke and its suggested extent (black and white arrows) based on the diagnostic three strips discussed in the text. Total dyke length is estimated to be 5,500 km. Dry season, θ = 21.5°, 30*10 m/pixel*

The best combination of bands for Envisat/ASAR image of the Mendoka dyke area (Fig. 9) does not succeed in identifying the dyke, due to the coarse resolution of ASAR.

On PALSAR quad-pol with HH polarization, the dyke appears as 3 parallel strips (Fig. 10). The central strip is dark, and is interpreted to be the dyke. The external strips are bright, and are thought to express the backscatter of the debris slopes. Because of the dry season, it seems clear that dyke and debris slope backscatter is dominated by roughness. The lower dyke backscatter is probably due to a block size two to three times larger than band L wavelength (23.6 cm), whereas band L wavelength is right in the size range of the debris slopes blocks.

The trails observed on the Spot P image (Fig. 8) are almost not visible because they are trampled, smooth zones blended with the dark image background.

The best image has been obtained by multiplying the HH and VV polarizations (Fig. 11). Fig. 10 and 11 suggest that the Mendoka dyke is actually longer than its extent within the white box. Two possible dyke segments are observed (arrows on Fig. 11), of cumulated length 5,500 km. Dyke extension northwestward and southeastward of the area displayed on Fig. 11 was sought-after but not found, based on the 3 diagnostic strips.

The interpretation of a length of 5,500 km can be checked by solving Eq. (2) for maximum thickness, given the 5-6 m dyke thickness measured in the field (it was measured on a single spot and may not represent the maximum thickness). A maximum thickness of 6.5 m is found, which is consistent with the field measurement. Conversely, in considering that the dyke does not extend further than its length observed within the white box (1 km), Eq. (2) would predict a maximum thickness of 2.8 m only, twice less than the thickness measured in the field. The interpretation given on Fig. 11 is therefore considered to be mechanically consistent and plausible.

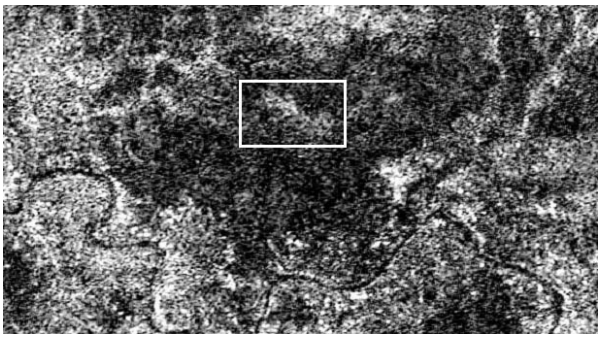

*Figure 12. PALSAR 4-POL HV/VH image of the Mendoka dyke area. Dry season, θ = 21.5°, 30*10 m/pixel*

Although the Mendoka dyke is observed in cross-polarization, the 3 diagnostic strips are not as clearly identified as on the HH and VV modes (Fig. 12).

The Mendoka dyke is also observed on FBD HH and HV polarization images, but they lack the diagnostic strips (Fig. 13).

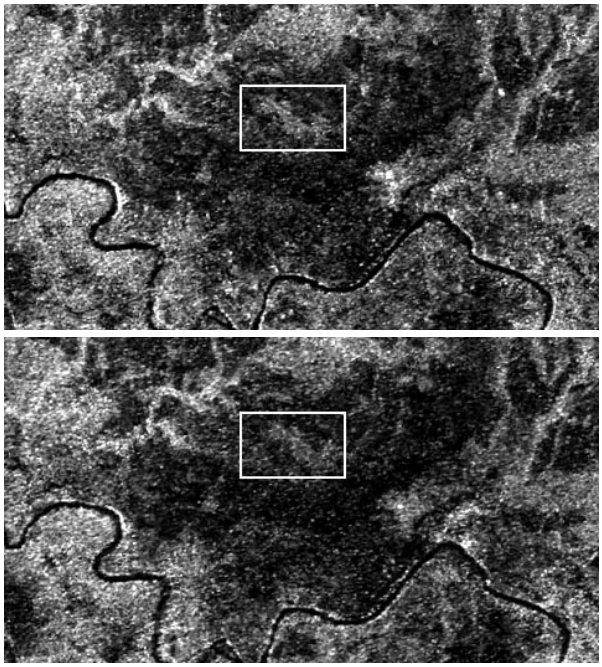

*Figure 13. PALSAR FBD HH (top) and HV(bottom) images of the Mendoka dyke area. Early wet season, θ = 34.3°, 19.5*10 m/pixel*

The FBD data were taken 22 days after the quad-pol data (June 27 and 5, 2007). The difference in basckscatter on Fig. 13 and Figs. 10-12 within the bed of river Ayma, the large river on the lower half of the images, shows that the rainy season has started between these two dates. Radar backscatter on Fig. 13 is therefore expected to be dominated by moisture and vegetation rather than roughness, despite the higher incidence angle than the incidence angle of the quad-pol images.

The FBS (HH) image enhances dyke sharpness due to a higher resolution higher than the resolution of the other polarization modes. Curiously, however, despite the image was taken during the dry season, the northern segment of the Mendoka dyke is not diagnostic in that the dyke and the debris slopes have the same backscatter intensity (Fig. 14). All the Palsar images used here were obtained in ascending mode, the main difference between the FBS and quad-pol data is therefore the incidence angle. An explanation for the globally less distinct diagnostic dyke signature may be that at θ = 21.5°, backscatter intensity is higher than at 34.3°, and roughness is mapped at the scale of small blocks, which is suitable for the debris slopes. At

θ = 34.3°, the global backscatter intensity is lower, and is more appropriate for mapping roughness at the scale of larger blocks. With this angle, the strongest backscatter would be obtained from both the largest debris slope blocks and the smallest dyke blocks, homogenizing the backscatter intensity of the dyke and debris slopes. More work is required, however, to evaluate this hypothesis.

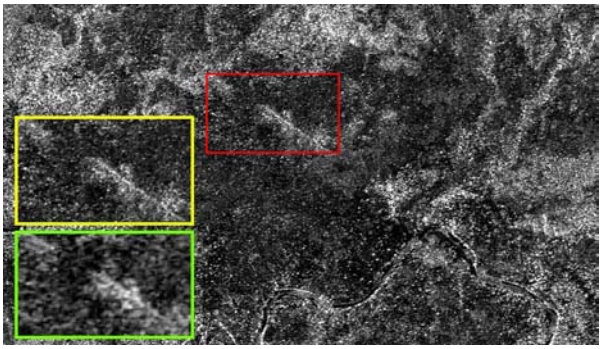

*Figure 14. PALSAR FBS image of the Mendoka dyke area. The area in the red box is enlarged in the yellow box. The green box displays an excerpt of the quad-pol image of the same area. Dry season, θ = 34.3°, 9.5*10 m/pixel*

4. DYKE #2

Fig. 15 shows a NNE-trending silicic dyke, rather similar to, though smaller than the Serpent dyke (Fig. 3). For this dyke SIR-C and Envisat/ASAR data are available for comparison with PALSAR. Its topography is much higher than the topography of the Mendoka dyke, except in areas where it is cut by a river. Debris slopes have also a steeper, gravity profile (~30°).

The three diagnostic bright-dark-bright strips are also observed for this dyke. However, this pattern is observed on the FBS image only. The Envisat/ASAR image (Fig. 16, North is to the upper right), in band C, succeeds in mapping dyke continuity in many places, though not everywhere. The diagnostic strips are observed, but not clearly enough to identify the dyke without any complementary data.

Although the diagnostic strips are not observed, the SIR-C images (Figs. 17-18) are excellent at tracing dyke continuity, locally better than both PALSAR and ASAR. Some dyke segments are better imaged in band C and others in band L. However, band C maps all the 2 dyke segments of Fig. 19 over their entire length, whereas one of the segment is incompletely mapped in band L.

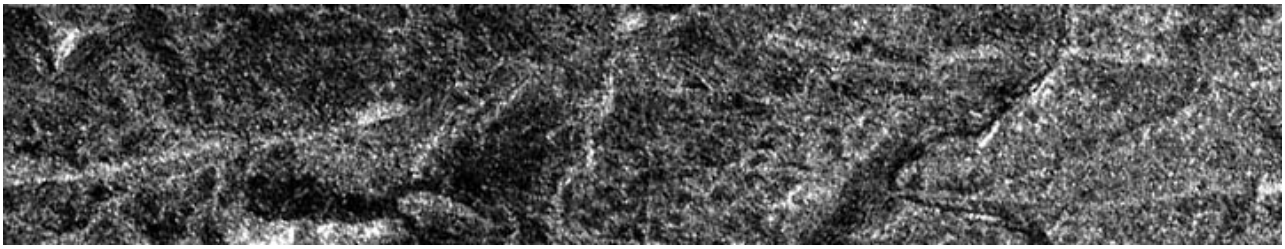

*Figure 15. PALSAR FBS image (HH) of the studied silicic dyke. Dry season, θ = 34.3°, 9.5*10 m/pixel, ascending orbit*

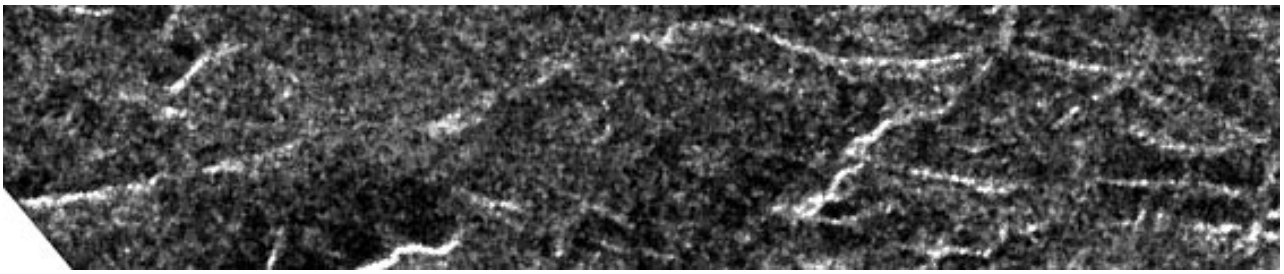

Figure 16. Envisat/ASAR image (VV) of the studied silicic dyke. Band C, Dry season, θ = 19-27°, 30 m/pixel, descending orbit

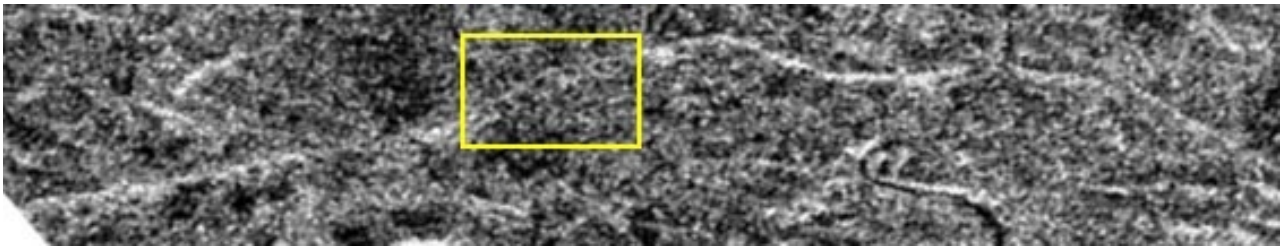

Figure 17. SIR-C image (HH+HV/2) of the studied silicic dyke. Band C, dry season, θ = 48.2°, 25 m/pixel, ascending orbit

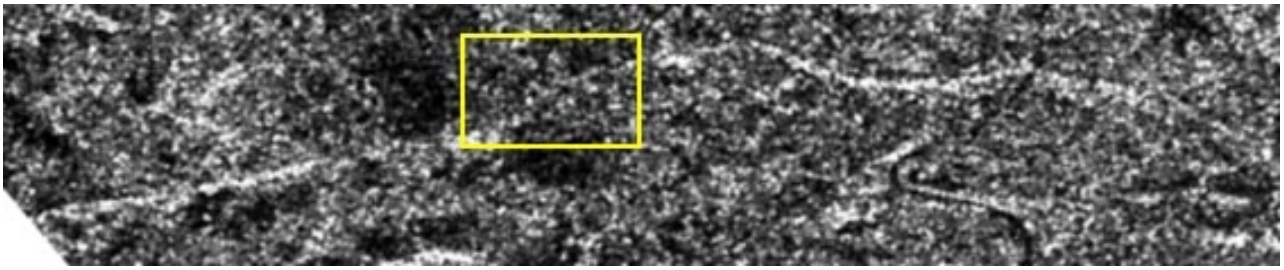

Figure 18. SIR-C image (HH+HV/2) of the studied silicic dyke. Band L, dry season, θ = 48.2°, 25 m/pixel, ascending orbit

Both the PALSAR and SIR-C images are in ascending mode, and were taken toward the end of the dry season. Excellent dyke continuity on SIR-C probably results in a large part from the high incidence angle.

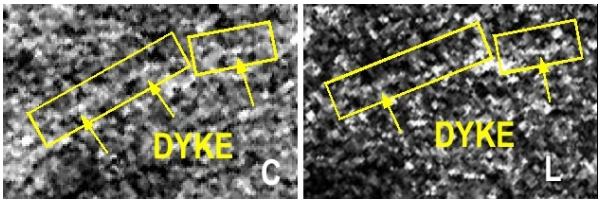

Figure 19. Enlargement of the yellow box of Figs 17 (left) and 18 (right).

5. CONCLUSION

Because the cumulated distribution of dyke length, and consequently thickness, follows a negative power law, many dykes can be imaged with Palsar that could not be detected with the previously available datasets, of coarser resolution. This improvement is significant in that for the first time a criterion for discriminating dykes from other linear patterns on radar imagery could be found. However, in turn, any future radar sensor having an enhanced resolution compared to Palsar should very significantly improve dyke detectability and identification.

Dykes can be unequivovally identified on PALSAR imagery by adjacent bright-dark-bright strips, corresponding to roughness contrasts between the dyke, its debris slopes, and the surrounding areas. This study has shown that observation of these strips under erosional conditions similar to those prevailing in the western Ethiopian volcanic province requires (1) that the images be taken during the dry season for the backscattered signal not to be dominated by moisture and/or vegetation; (2) HH and/or VV polarization (both if possible). In the quad-pol mode, HV and VH are not useful by themselves for identifying dykes, nevertheless, because of groundwater trapping by dykes at depth, the vegetation component of dyke signal is potentially useful to study and understand. For this reason, identification of dykes using quad-pol is encouraged.

While the FBS mode is mandatory for increasing the sharpness of dykes, it was found to be more appropriate to identify unequivolcally the silicic dyke using the three roughness strips criterion than the basaltic dyke. More work is required, however, to check whether this observation can be generalized to the silicic and basaltic dyke populations in the study area.

From SIR-C data, it does not appear obvious that band L is always better than band C to detect dykes, an assertion frequently made when dealing with geological interpretations of SAR data. More work on dykes is also required to investigate this issue further. Moreover, SIR-C data are presently not obsolete for tracing dyke continuity, probably due to SIR-C's high incidence angle.

Especially critical in dyke identification is how dyke and debris slope roughness are imaged. The erosional processes acting on dykes result in a roughness at a different scale for a dyke and its debris slopes. Consequently, the most appropriate sensor, with a resolution even higher than PALSAR, would permit a combination of wavelength (C or L) and incidence angle (20 to 50° as a first approximation) that is flexible enough for distinguishing roughness at various scales, from centimeters to 1 meter.

6. ACKNOWLEDGEMENTS

This work has been carried out within the framework of ALOS/ADEN project 3561. The ESA ADEN node is warmly thanked for granting access to the Alos, Envisat, and Spot data used in this preliminary study, and the EOHelp desk for rapid and helpful support for any kind of data-related issues. CNRS/INSU and the University of Nantes have funded various segments of this work. Tewodros Rango (University of Ferrara), is thanked for his contribution to field work at the Mendoka dyke, and Tesfaye Korme (Regional Center for Mapping of Resources for Development, Nairobi) for his contribution to field work at the other dyke. Dykes are thanked for being dykes.

7. REFERENCES

1. Mège, D. & Korme, T. (2004a). Dyke Swarm Emplacement in the Ethiopian Flood Basalt Province: Not only a Matter a Stress. *J. Volcanol. Geotherm. Res.* **132**, 283-310.

2. Wignall, P.B. (2001). Large Igneous Provinces and Mass Extinctions. *Earth-Sci. Rev.* **53**, 1-33.

3. Heydari, E., Arzani, N. & Hassanzadeh, J. (2008). Mantle Plume: The Invisible Serial Killer, Application to the Permian-Triassic Boundary Mass Extinction. *Palaeogeography, Palaeoclimatology, Palaeoecology* **264**, 147-162.

4. Babiker, M. & Gudmundsson, A. (2004). The Effect of Dykes and Faults on Groundwater Flow in an Arid Land: the Red Sea Hills, Sudan. *J. Hydrol.* **297**, 256-273.

5. Mège, D. & Rango, T. Permanent groundwater storage in basaltic dyke fractures and termite mound viability. Submitted to *J. Afr. Earth Sci.*, 2008.

6. Mège, D. & Korme, T. (2004b). Fissure Eruption of Flood Basalts from Statistical Analysis of Dyke Fracture Length. *J. Volcanol. Geotherm. Res.* **131**, 77-92.

7. Wada, Y. (1994). On the Relationship between Dike Width and Magma Viscosity. *J. Geophys. Res.* **99**, 17,743-17,755.

8. Schultz, R.A., Mège, D. & Diot, H. (2008). Emplacement conditions of igneous dikes in Ethiopian Traps. *J. Volcanol. Geotherm. Res.*, in press.

9. Olson, J. (2003). Sublinear Scaling of Fracture Aperture versus Length: An Exception or the Rule? *J. Geophys. Res.* **108**, 2413, doi:10.1029/2001JB000419.

10. Jaeger, J. C. (1968). Cooling and solidification of igneous rocks. In *Basalts, the Poldervaart Treatise on Rocks of Basaltic Composition, vol. 2* (Eds. H. H. Hess and A. Poldervaart), Wiley & Sons, New York, pp503-536.